Dental Materials Journal 2025; 44(2): 146–156

Mechanical and structural characterization of CAD-CAM materials and enamel of deciduous and permanent teeth

Kanae WADA[1,2], Sufyan GAROUSHI[1], Junichiro WADA[1,3], Tsutomu IWAMOTO[2], Pekka K. VALLITTU[1,4] and Lippo LASSILA[1]

[1] *Department of Biomaterials Science and Turku Clinical Biomaterials Centre —TCBC, Institute of Dentistry, University of Turku, Lemminkaisenkatu 2, FI-20520 Turku, Finland*
[2] *Department of Pediatric Dentistry/Special Needs Dentistry, Institute of Science Tokyo, 1-5-45 Yushima, Bunkyo-ku, Tokyo 113-8510, Japan*
[3] *Department of Advanced Prosthodontics, Institute of Science Tokyo, 1-5-45 Yushima, Bunkyo-ku, Tokyo 113-8510, Japan*
[4] *Welfare District of South-West Finland, FI-20520 Turku, Finland*
Corresponding author, Kanae WADA; E-mail: wadadohs@tmd.ac.jp

In clinical applications, computer-aided design/computer-aided manufacturing (CAD-CAM) blocks must exhibit behavior similar to that of deciduous teeth. The purpose of this study was to evaluate the material properties and suitability of CAD-CAM as deciduous teeth. Experimental fiber-reinforced CAD-CAM composites (FRC) and various CAD-CAM (lithium disilicate ceramic: IPS, hybrid ceramic: VEM, five composite resins, and PMMA) and enamels (deciduous and permanent teeth) were subjected to nanoindentation to evaluate material properties, including nanohardness and nano-reduced elastic modulus. Energy dispersive X-ray spectrometry was conducted in combination with SEM to evaluate the elemental and microstructural properties. FRC-fiber (2.94 GPa), VEM-ceramic (3.20 GPa), and IPS (3.63 GPa) showed no statistically significant differences compared to deciduous enamel (3.37 GPa). Various CAD-CAM materials were confirmed to exhibit sufficient nanohardness and nano-reduced elastic modulus and a strong microstructure, indicating their potential for application in the restorative treatment of full crowns of deciduous teeth.

Keywords: Deciduous enamel teeth, CAD-CAM materials, Nanoindentation, Nanohardness, Nano reduced elastic modulus

INTRODUCTION

With the development of digital technology, expectations for full-crown restorations using highly esthetic computer-aided design/computer-aided manufacturing (CAD-CAM) blocks in pediatric dentistry are growing. In the clinical application of materials, various aspects such as mechanical properties, adhesion, and wear resistance must be considered. To improve clinical prognosis, CAD-CAM blocks, which have a higher risk of fracture and detachment than metals, should exhibit behavior similar to that of deciduous teeth after restoration. However, studies on their application in the restorative full crown treatment of deciduous teeth are limited.

Stainless steel crowns (SSCs) have been widely used for effective full-crown restorations of severely carious deciduous molars, especially those receiving endodontic treatment, owing to their high strength and long-term durability[1]. However, there is an increasing demand for the esthetic restoration of deciduous teeth, including molars[2,3]. Prefabricated pediatric zirconia crowns have been used in pediatric dentistry clinics in recent years and are an esthetically pleasing alternative for the restoration of deciduous molar teeth[4]. However, zirconia crowns exhibit greater hardness than conventional SSCs[5] and may lead to the wear of antagonist teeth[6]. Alternative esthetic restorations using three-dimensional (3D)-printed materials for the crown restoration of deciduous teeth have been investigated[7]; however, they have not yet been applied in practical cases.

CAD-CAM materials available for dental restorations include lithium disilicate ceramics, hybrid ceramics, and composites. Lithium disilicate ceramics are widely used in indirectly bonded permanent prosthetics owing to their remarkable esthetic and mechanical performance. Concurrently, with the development of ceramic materials for CAD-CAM, considerable progress has been made in the development of nanohybrid and nano-filled CAD-CAM composites[8]. Because CAD-CAM composite crowns are fabricated under manufacturing conditions such as heat curing, they demonstrate stability in their physical properties[9]. Yamaguchi *et al*. concluded that CAD-CAM composite molar crowns containing nanofillers with a higher fraction of a resin matrix exhibited higher fracture loads and greater longevity. This suggests that these crowns could be used as alternatives to ceramic crowns because of their higher fatigue resistance[10]. Wada *et al*. studied the effects of materials with different hardnesses and wear properties on deciduous teeth, and reported that composite resins are less likely to cause wear on antagonist deciduous teeth[2,11]. Recently, short-fiber-reinforced CAD-CAM composites (SFRC CAD) have been developed to improve the fracture toughness[12-14].

Predicting the clinical success of deciduous tooth materials is important for evaluating their mechanical properties, such as the modulus of elasticity[15-17] and hardness related to wear resistance[2,18,19]. The degradation of composite resins involves the leaching of elements[20] and changes in the chemical composition from leaching[21]. Therefore, the appropriate mechanical properties and elemental composition of the material must be evaluated to predict its long-term durability

Received Aug 1, 2024: Accepted Nov 5, 2024
doi:10.4012/dmj.2024-245 JOI JST.JSTAGE/dmj/2024-245

in the oral environment. However, to the best of our knowledge, only a few studies have evaluated the mechanical properties and conducted elemental analyses of various CAD-CAM materials, including experimental fiber-reinforced CAD-CAM composites, lithium disilicate ceramics, hybrid ceramics, composites, polymethyl methacrylate (PMMA), and compared them to deciduous tooth enamel. Therefore, the purpose of this study was to evaluate the suitability of various CAD-CAM blocks for the crown restoration of deciduous teeth from various angles. This study focused on the evaluation of nanohardness and nano-reduced elastic modulus, elemental analyses, and clarification of the differences between deciduous and permanent teeth.

MATERIALS AND METHODS

Materials and specimen preparation

The nine different CAD-CAM materials used in this study were the experimental fiber-reinforced resin block (FRC), lithium disilicate ceramic block (IPS e.max CAD), hybrid ceramic block (VITA ENAMIC), composite resin blocks (KZR-CAD HR Block 2 plus, CERASMART 270, CERASMART 300, KATANA AVENCIA Block 2, Paradigm MZ 100 Block), and PMMA-based block (PMMA BLOCK). Enamel was used from deciduous and permanent teeth. A list of the materials studied, with details of the monomer and filler contents, is provided in Table 1.

Table 1 Materials used in this study

Material	Code	Composition			Manufacturer	Type
		monomer	Filler	Mass wt%		
IPS e.max CAD	IPS	—	SiO_2, Li_2O, other oxides	68–99	Ivoclar Vivadent, Schaan, Liechtenstein	Lithium disilicate ceramic
VITA ENAMIC	VEM	UDMA, TEGDMA, feldspar ceramic enriched with aluminum oxide	SiO_2, Al_2O_3, Na_2O, K_2O, B_2O_3, ZrO_2, CaO	86	Vita Zahnfabrik, Bad Sackingen, Germany	Hybrid ceramic
FRC Experimental	FRC	UDMA, TEGDMA	Short glass fiber (200–300 μm& Ø7 μm), barium glass	77	Stick Tech, GC member, Turku, Finland	Fiber reinforced resin
KATANA AVENCIA Block 2	KTA	methacrylate monomer	SiO_2 (40 nm), Al_2O_3 (20 nm)	60	Kuraray Noritake Dental, Tokyo, Japan	Resin composite
Paradigm MZ 100 Block	PZB	Bis-GMA, TEGDMA	Zirconia-silica ceramic	85	3M ESPE, St Paul, MN,USA	Resin composite
KZR-CAD HR Block 2 plus	KZR	UDMA, TEGDMA	SiO_2 (20 nm), aggregated SiO_2–Al_2O_3–ZrO_2 (200– 600 nm), fluoride sustained release filler (700 nm), cluster (1–20 μm)	72	Yamakin, Osaka, Japan	Resin composite
CERASMART 270	C27	UDMA, Bis-MEPP, DMA	Silica (20 nm), Barium glass (300 nm)	71	GC, Tokyo, Japan	Resin composite
CERASMART 300	C30	UDMA	Barium glass	75	GC	Resin composite
PMMA BLOCK	PMM	PMMA, EDMA	—	—	Yamahachi Dental, Aichi, Japan	PMMA-based
Primary molar enamel	PME	—	—	—	—	Enamel
Deciduous molar enamel	DME	—	—	—	—	Enamel

Bis-GMA: bisphenol A-glycidyl methacrylate, UDMA: urethane dimethacrylate, TEGDMA: triethylene glycol dimethacrylate, EDMA: ethylene glycol dimethacrylate, Bis-MEPP: 2,2-bis (4-methacryloxypolyethoxyphenyl) propane, DMA: dimethacrylate, wt%: weight percentage

Each CAD-CAM material was sectioned (10 mm long×14 mm wide×3 mm thick) into plates using a diamond blade (Secotom-50, Struers, Cleveland, OH, USA) mounted on a saw (10S20, Struers) under constant water irrigation. Seven CAD-CAM blocks were prepared (Fig. 1a). IPS did with sintering process. Each six specimens of these blocks were wet ground and polished with a lapping machine (LaboPol-21, Struers) with a series of silicon carbide papers (SiC) and paper disks P320, P500, P1200, P2400, and P4000-grit (Exakt Technologies, Oklahoma City, OK, USA) under water cooling and then polished with 0.25 μm silica polishing paper (OP-S, Struers, Ballerup, Denmark), followed by gentle cleansing using an ultrasonic cleaning unit (Quantrex® 90, L&R Ultrasonics, Kearny, NJ, USA) with distilled water for 5 min. The specimens were then dried for 24 h at room temperature.

Permanent enamel (PME) discs were fabricated from extracted wisdom teeth, and deciduous enamel (DME) discs were prepared from the second deciduous molars that had been removed during the replacement phase. The study was conducted in accordance with the guidelines of the Declaration of Helsinki and approved by the Ethics Committee of Tokyo Medical and Dental University (D069-01). No personal data were collected from the patients. Two permanent teeth and two deciduous molars were used, and the enamel of each tooth was embedded in a block of a self-curing acrylic resin, which was cut parallel to its long axis with a diamond saw to create four blocks (n=4). The sample size was determined by referring to previous study[22]. The surface of the sectioned material was ground with #4,000, 0.25 μm silica polishing paper (Fig. 1b). The samples were stored in ethylene glycol (YA Kemia, Helsinki, Finland) for 12 h to avoid excessive drying during testing[22].

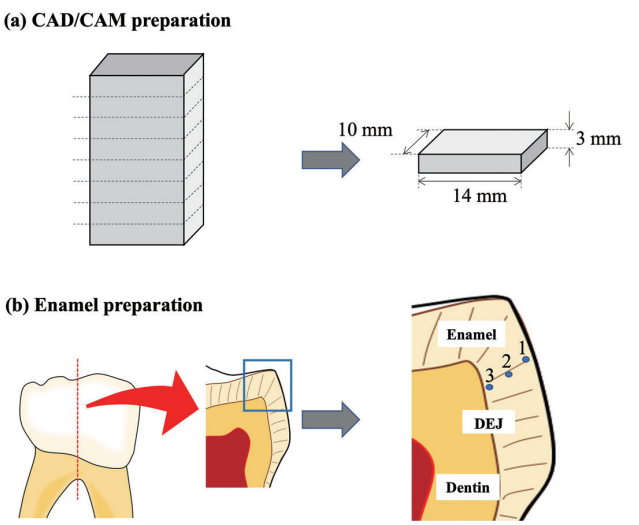

Fig. 1 (a) CAD-CAM blocks of the same size and thickness were prepared by cutting. (b) Each tooth was embedded in a block of a self-curing acrylic resin and cut parallel to the long axis with a diamond saw. DME and PME measurements were conducted by dividing the enamel into three layers of the same thickness, from the outermost to innermost layer.

Nanoindentation testing

1. Wide range of measurements

To measure the nanohardness (GPa) and nano-reduced elastic modulus (GPa), nine types of CAD-CAM blocks were tested 11 times for each sample (n=6) at a maximum force of 8 mN, and the average was calculated. For enamel (DME and PME) analyses, the enamel was divided into three layers of the same thickness, from the outermost to innermost layer, and each layer was measured 11 times. Thirty-three measurements (n=4) were performed for each specimen, and the average was calculated (Fig. 1b).

2. Narrow point area of measurement

Narrow-range measurements were conducted for the VEM and FRC samples. The materials used were VEM-measured ceramic and polymer (VEM-ceramic and VEM-polymer, respectively), and FRC-measured fiber and matrix (FRC-fiber and FRC-matrix, respectively) areas. In preliminary experiments, the VEM and FRC samples were found to have distinctly different properties in terms of fillers and polymers of different colors. Therefore, to determine the material properties over a range, we randomly mapped the material properties from the regions of the filler and polymer with different colors from a given region. For the number of indentations, one sample was taken 11 times (n=6) from the filler area and 11 times (n=6) from the polymer and matrix areas.

Nanoindentation measurements (*i.e.*, nanohardness and nano-reduced elastic modulus measurements) were conducted using a nanoindenter (UBi1 TI-750, Hysitron, Minneapolis, MN, USA) equipped with a 90° cube corner diamond tip on a fused quartz tip, which was used with indenter. Using the TriboScan software (version 9.1.1.0, Hysitron), nanohardness and nano-reduced elastic modulus were calculated using the following equations:

$$NH = \frac{P}{A_i}$$

where NH is the nanohardness (GPa), P is the applied load (N) and A_i is the projected area of indentation.

$$\frac{1}{E^*} = \frac{1-\upsilon^2_m}{E_m} + \frac{1-\upsilon^2_i}{E_i}$$

where E^* is the reduced elastic modulus (GPa), υ_m is the Poisson's ratio of the material, E_m is the elastic modulus of the material (GPa), υ_i is the Poisson's ratio of the indenter, and E_i is the elastic modulus of the indenter.

Nanoindentation was performed using a nanoindentation system (Tri-bo Scope, Hysitron) in combination with *in situ* scanning probe microscopy (SPM). After the nanoindentation test, the indentation area was scanned through *in situ* SPM. Cross-sectional analysis was also conducted to analyze the indentation imprints to understand the mechanical behavior of the

CAD-CAM material impacted by the diamond indenter. Figure 2 shows the two-dimensional (2D) and 3D SPM images of nanoindentation imprints exhibiting plastic deformation.

Microstructure analysis through scanning electron microscopy (SEM) and elemental analyses via energy dispersive X-ray spectrometry (EDS)

The surface of each group was examined through SEM (LEO Gemini 1530, Carl Zeiss, Oberkochen, Germany) with backscattered election at 10,000× magnification and 20 kV.

For elemental analysis, each sample (n=1) was gold sputtered for EDS, and nine CAD-CAM blocks and enamels were analyzed over a wide range and narrow point area. Elemental analysis was performed to determine the elemental composition of the filler particles using a field-emission electron probe microanalyzer (UltraDry detector, Thermo Scientific, Madison, WI, USA). Wide-range analysis was performed at a voltage of 20 kV, an image pixel size of 4.06 μm, and a low magnification (30×). For the four CAD-CAM blocks (VEM, FRC, KZR, and KTA), narrow point area measurement was performed at a voltage of 20 kV, an image pixel size of 0.01 μm, and a high magnification (10,000×) for filler spot point and monomer area analysis. Analyses were performed for each group, and typical data were employed as representative values.

Statistical analysis

The Kolmogorov–Smirnov test confirmed that the acquired data (nanohardness and nano-reduced elastic modulus) were not normal. Therefore, the nanohardness and nano-reduced elastic modulus were statistically analyzed using the Kruskal–Wallis test, followed by pairwise comparison using the Mann–Whitney U test with Bonferroni correction. Statistical analyses were performed using a statistical software (SPSS ver. 28.0, IBM, Armonk, NY, USA), with the significance level set at 0.05. To confirm the correlation between the nanohardness and nano-reduced elastic modulus of the CAD-CAM materials, Spearman's correlation coefficient (ρ) was calculated for the nine materials combined.

RESULTS

Nanoindentation testing

The mean nanohardness and nano-reduced elastic modulus of all tested specimens are shown in Figs. 3a and b, and the relationship between the nanohardness and nano-reduced elastic modulus of the various materials is shown in Fig. 3c. Statistically significant differences in the mean nanohardness and nano-reduced elastic modulus were observed between the tested specimens. Measurements are separately shown, in which the VEM measurements were divided into the ceramic (VEM-ceramic) and polymer matrix (VEM-polymer), and the FRC measurements were divided into the fiber (FRC-fiber) and surrounding matrix (FRC-matrix). In addition, FRC-fiber was measured by dividing the directionality into cross (FRC fiber-cross) and horizontal (FRC fiber-horizontal) sections. The median and interquartile range (IQRs) of the nanohardness ranged from PMM (median, 0.29 [IQR, 0.005] GPa) to PME (median, 4.34 [IQR, 0.4] GPa). The ranking of nanohardness figures was as follows: PME (4.34[0.4])>IPS (3.63[0.105])>DME (3.37[0.58])>VEM-ceramic (3.20[0.105])>FRC fiber-horizontal (2.94[0.095])>FRC fiber-cross (2.84[0.04])>VEM-polymer (1.08[0.085])>KTA (1.03[0.015])>PZB (0.72[0.0425])>C27 (0.72[0.0345])>KZR (0.71[0.0345])>FRC-matrix (0.66[0.042])>C30 (0.65 [0.0135])>PMM (0.29[0.005]). No significant differences were observed between the DME and PME groups. There were no statistically significant differences among DME, PME, IPS, VEM-ceramic, and FRC-fiber. In addition, there were no statistically significant differences among DME, VEM-polymer, and KTA. DME and PME showed significantly

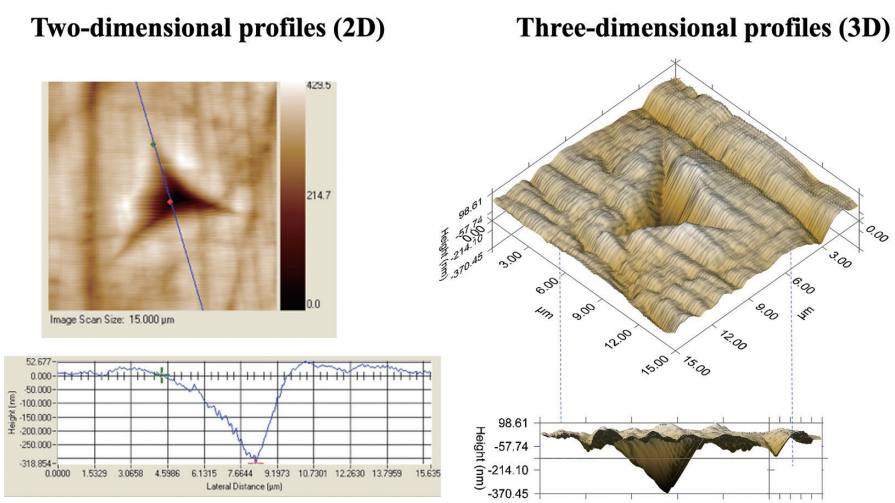

Fig. 2 2D and 3D SPM images of the nanoindentation imprints exhibiting plastic deformation.

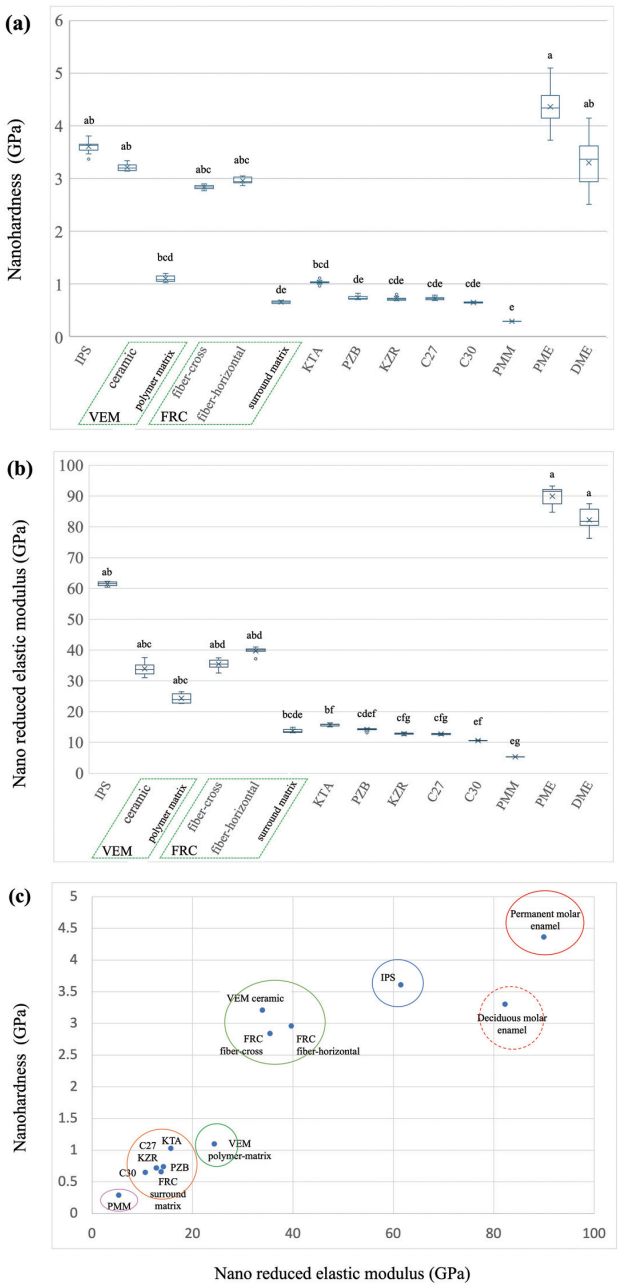

Fig. 3 Box and whisker plots of (a) nanohardness (standard deviation) and (b) nano-reduced elastic modulus. The horizontal black line in the box stands for the median. The same superscription indicates the groups showing no statistically significant difference. (c) Relationship between nanohardness and nano-reduced elastic modulus of various materials.

higher nanohardness than the FRC-matrix (p<0.001), PZB (p<0.001), KZR (p<0.001), C27 (p<0.001), C30 (p<0.001), and PMM (p<0.001) matrices. The properties of VEM-polymer and FRC-matrix were not significantly different from those of the composite resins.

The nano-reduced elastic modulus values ranged from median 5.28 [IQR, 0.06] GPa (PMM) to median 91.50 [IQR, 4.44] GPa (PME). The order of the nano-reduced elastic modulus figures was as follows: PME (91.50[4.44])>DME (81.78[4.39])>IPS (61.59[1.085])>FRC fiber-horizontal (39.98[0.49])>FRC fiber-cross (35.46[2.015])>VEM-ceramic (33.65[2.15])>VEM-polymer (23.89[2.27])>KTA (15.78[0.47])>PZB (14.27[0.265])>FRC-matrix (13.48[0.665])>KZR (12.82[0.315])>C27 (12.77[0.275])>C30 (10.56[0.12])>PMM (5.28[0.06]). No significant differences were observed between the DME and PME groups. There were no statistically significant differences between the DME, PME, IPS, VEM, and FRC-fiber. DME and PME showed significantly higher nano-reduced elastic moduli than the FRC-matrix (p<0.001) and composite resin groups [KTA (p<0.001), PZB (p<0.001), KZR (p<0.001), C27 (p<0.001), C30 (p<0.001), and PMM (p<0.001)]. VEM-polymer and FRC-matrix were not significantly different from the composite resin groups.

There was a high correlation (ρ=0.813, p<0.001) between the nanohardness and nano-reduced elastic modulus of the CAD-CAM materials (Fig. 3c). The nanohardness and nano-reduced elastic modulus of VEM differed significantly between the ceramic and polymer areas, whereas those of FRC differed significantly between the fiber and matrix areas.

SPM images of nanoindentation imprints

All indentations in each group exhibited plastic deformation, as evidenced by crack-free indentation edges and corners with stress concentrations. Figure 4 shows the typical 2D scanning cross-sectional profile images. Plastic pile-ups of approximately 7.7–138.01 nm occurred around these indentation contacts. The plastic pile-ups of IPS tended to be the lowest (7.7 nm), whereas those of DME tended to be higher (138.01 nm). Stepped ridge indentation imprints are visible in the KTA, KZR, and PMM samples. Among the composite resin blocks, PZB tended to be smaller (22.6 nm). VEM-ceramic tended to be lower than that of FRC-fiber. Figure 5 shows the 2D and 3D SPM images of the DME with the highest plastic pile-up. Figure 6 shows the FRC-fiber and surrounding matrix 2D SPM images of the nanoindentation imprints after testing at 8 mN. Clearly, nanoindentation imprints of different sizes exist in the fiber and the surrounding matrix.

Microstructure analysis of SEM

The SEM images show the different microstructures of the nine tested CAD-CAM materials at 10,000× magnification and 20 kV (Fig. 7). It can be noticed that the CAD-CAM materials had versatile microstructural constituents as well as variable filler contents. IPS was characterized by matrix glass and dispersed two varieties of short and long 0.5–3-μm-sized cylinder-shaped particles of leucite crystals. VEM exhibited a dense ceramic network structure consisting of small ceramic particles and polymers matrix. KZR contained various <1 μm sizes of the filler. C27, C30, and FRC contained relatively large and small within 1 μm and uniformly

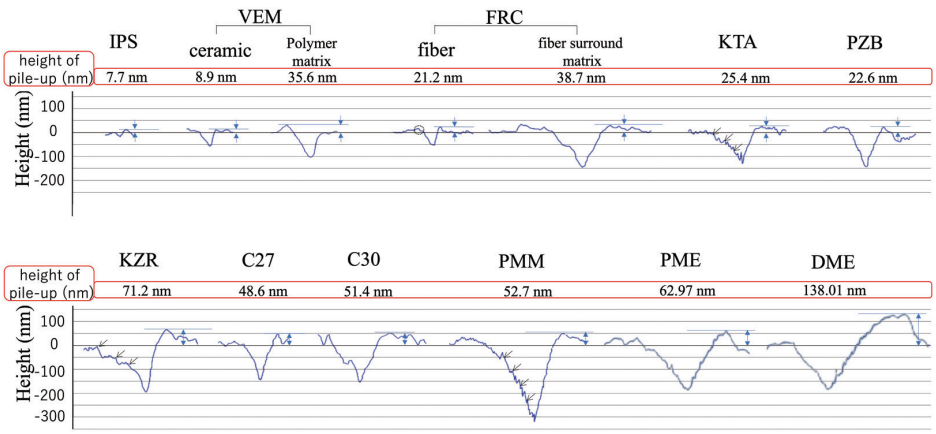

Fig. 4 Typical 2D scanning cross-sectional profiles images with plastic pile-ups of each specimen nanoindentation impressions.
The value indicates the plastic pile-ups and the arrows indicate the stepped ridges.

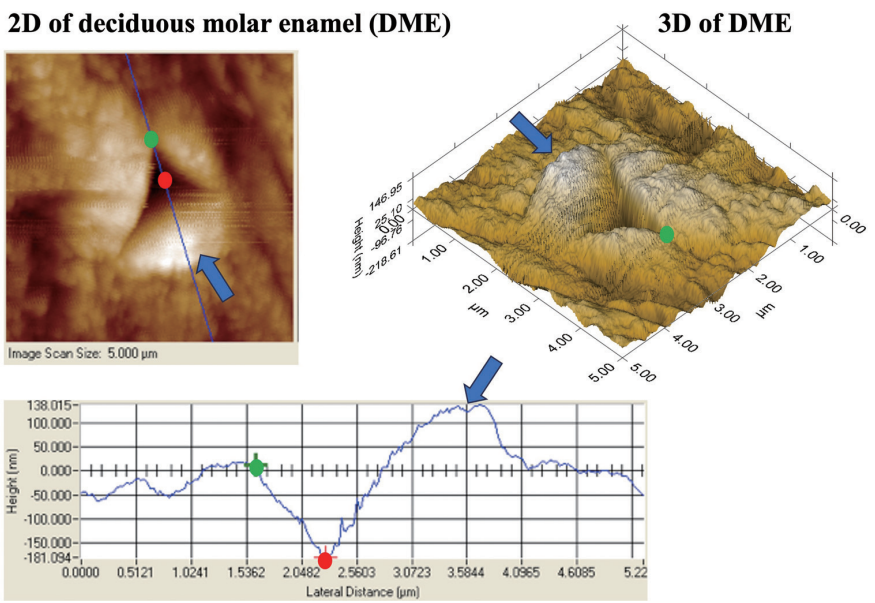

Fig. 5 2D and 3D SPM images of nanoindentation imprints exhibiting plastic deformation.
The arrows indicate the plastic pile-ups in DME.

distributed particles, and 10–50 µm short glass fiber of FRC was clearly visible in shape at 1,000× magnification in various directions (Fig. 7). KTA was characterized by a dense structure composed of methacrylate monomers, which occupied most of the area, and a few spherical filler particles with a diameter of approximately <1 µm. PZB contained a variety of 0.3–1.5-µm-sized spherical particles. PMM did not contain fillers.

Elemental analyses via EDS

The results of the range 30× magnifications at 20 kV elemental analysis of the CAD-CAM materials and enamels are shown in Fig. 8. C, O, and Si were detected in all materials. Al and Sr were detected in all materials except PMM. Mg, P, K, Zn, Zr, and Ce were detected in IPS. Na and K were detected in VEM. FRC, C27, and C30 showed similar trends for F and Ba; however, N, Mg, Cl, and Ca were also detected in FRC. N, F, Zn, and Zr were detected in the KZR specimens. For KTA, Cl and Ca were detected. Na, Ca, and Zr were also detected in PZB. Many types of elements were detected in IPS and FRC. C, O, Na, Mg, Al, P, and Ca were detected in PME and DME. The calcium to phosphorus (Ca/P) ratio was 1.67 wt% for PME and 1.79 wt% for DME.

Figure 9 shows the results of the elemental analysis of the filler and monomer narrow point area

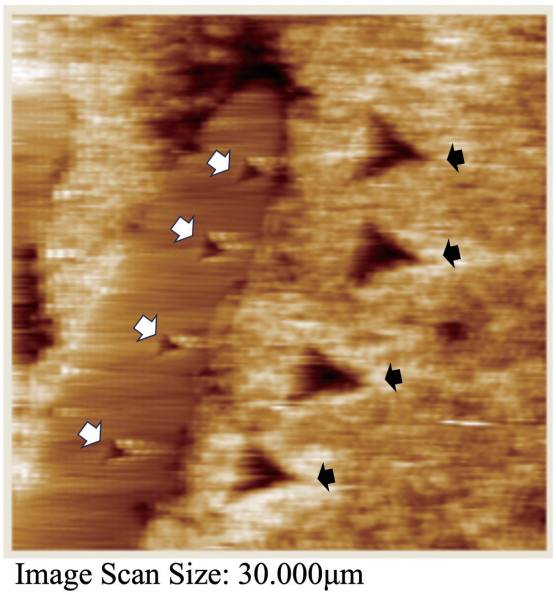

Fig. 6 Fiber and surround matrix of FRC 2D SPM images of nanoindentation imprints after testing at 8 mN. The white arrows indicate the imprints of the fiber and black arrows indicate the imprints of the surround matrix. The nanoindentation imprints of the fiber and surround matrix showed clearly different sizes.

at 10,000× magnification for VEM, KZR, and KTA and 1,000× magnification for FRC, revealing particular characteristics of the samples. For VEM, O was in the ceramic spot and C was detected in the polymer matrix area. For KZR, F and Sr were present in the filler spot, and C, N, and Zr were detected in the monomer area. For KTA, Ti was in the filler spot and Si was detected in the monomer area. For FRC, C, N, and Ba were in the filler spot, and Na, Mg, and Zr were detected in the fiber area.

DISCUSSION

IPS showed the highest values of nanohardness (3.63[0.105] GPa) and nano-reduced elastic modulus (61.59[1.085] GPa) among the materials, with no statistically significant difference for the nanohardness (3.37[0.58] GPa) and nano-reduced elastic modulus (81.78[4.39] GPa) of DME. The nanohardness values of VEM-ceramic (3.2[0.105] GPa) and FRC-fiber (2.94[0.095] GPa) were also relatively close to those of DME. In contrast, the VEM-polymer (1.08[0.085] GPa) and FRC-matrix regions (0.655[0.042] GPa) were similar to the composite resin group (0.647[0.0135]) GPa to 1.03[0.015] GPa). The nanohardness and nano-reduced elastic modulus values of DME and PME teeth were not significantly different. Therefore, various

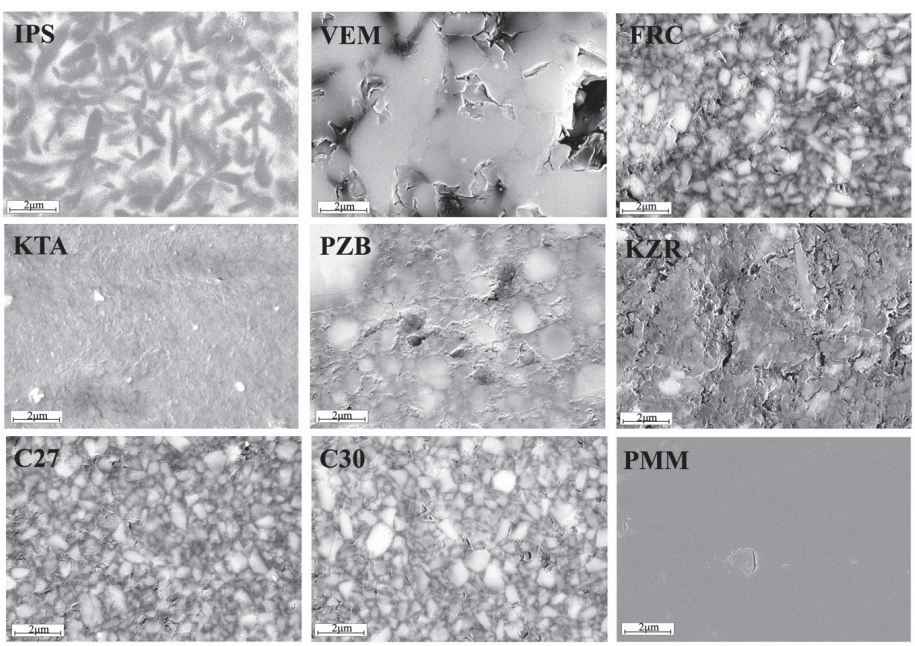

Fig. 7 SEM images of the CAD-CAM materials of the nine tested materials at 10,000× magnification at 20 kV.
IPS: two varieties of short and long 0.5–3-µm-sized cylindrical particles were observed. VEM: a dense ceramic network structure with a polymer matrix was present. KTA: a spherical filler, approximately 1 µm in diameter, was observed. PZB: small white spherical particles and large spherical particles were present. KZR: filler aggregates of various sizes were observed. C27, C30, and FRC: large and small with <1-µm-sized and uniformly distributed particles were present.

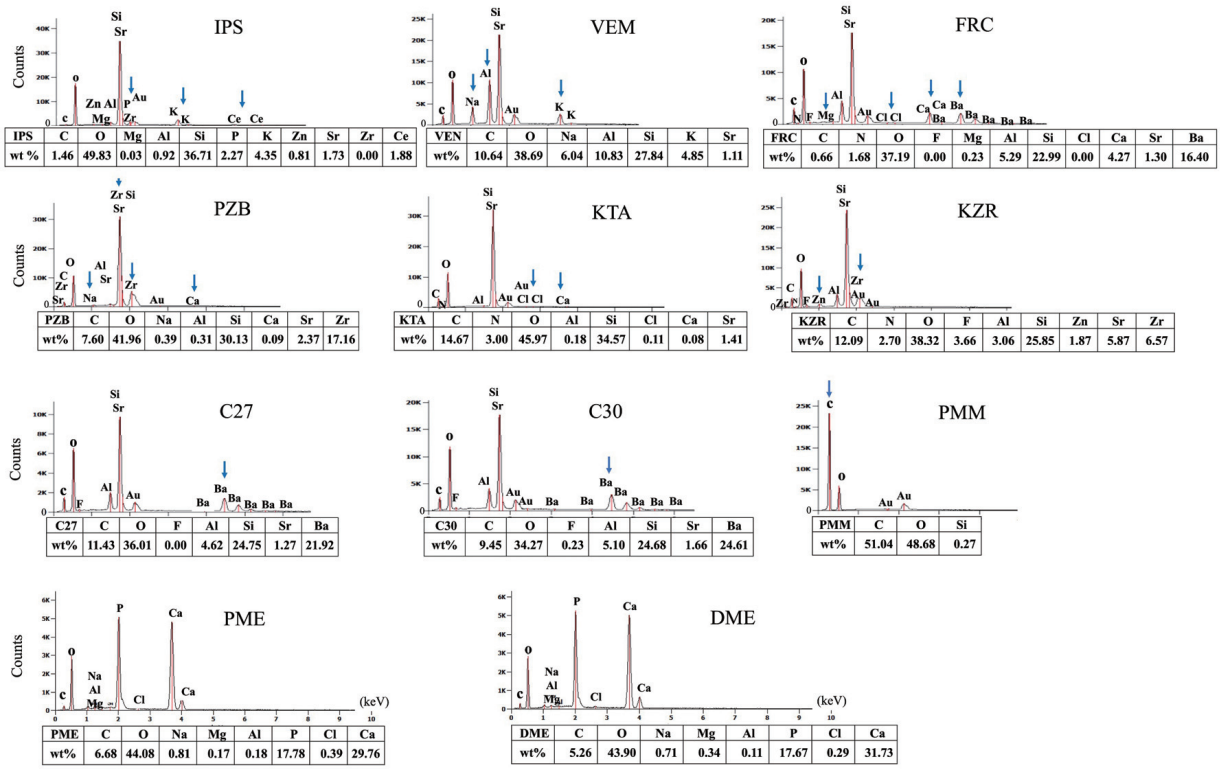

IPS	C	O	Mg	Al	Si	P	K	Zn	Sr	Zr	Ce
wt %	1.46	49.83	0.03	0.92	36.71	2.27	4.35	0.81	1.73	0.00	1.88

VEN	C	O	Na	Al	Si	K	Sr
wt%	10.64	38.69	6.04	10.83	27.84	4.85	1.11

FRC	C	N	O	F	Mg	Al	Si	Cl	Ca	Sr	Ba
wt%	0.66	1.68	37.19	0.00	0.23	5.29	22.99	0.00	4.27	1.30	16.40

PZB	C	O	Na	Al	Si	Ca	Sr	Zr
wt%	7.60	41.96	0.39	0.31	30.13	0.09	2.37	17.16

KTA	C	N	O	Al	Si	Cl	Ca	Sr
wt%	14.67	3.00	45.97	0.18	34.57	0.11	0.08	1.41

KZR	C	N	O	F	Al	Si	Zn	Sr	Zr
wt%	12.09	2.70	38.32	3.66	3.06	25.85	1.87	5.87	6.57

C27	C	O	F	Al	Si	Sr	Ba
wt%	11.43	36.01	0.00	4.62	24.75	1.27	21.92

C30	C	O	F	Al	Si	Sr	Ba
wt%	9.45	34.27	0.23	5.10	24.68	1.66	24.61

PMM	C	O	Si
wt%	51.04	48.68	0.27

PME	C	O	Na	Mg	Al	P	Cl	Ca
wt%	6.68	44.08	0.81	0.17	0.18	17.78	0.39	29.76

DME	C	O	Na	Mg	Al	P	Cl	Ca
wt%	5.26	43.90	0.71	0.34	0.11	17.67	0.29	31.73

Fig. 8 Elemental analysis of the nine CAD-CAM materials and PME and DME of the tested specimen at wide range under 30× magnification.
At 20 kV, detector; EDX.

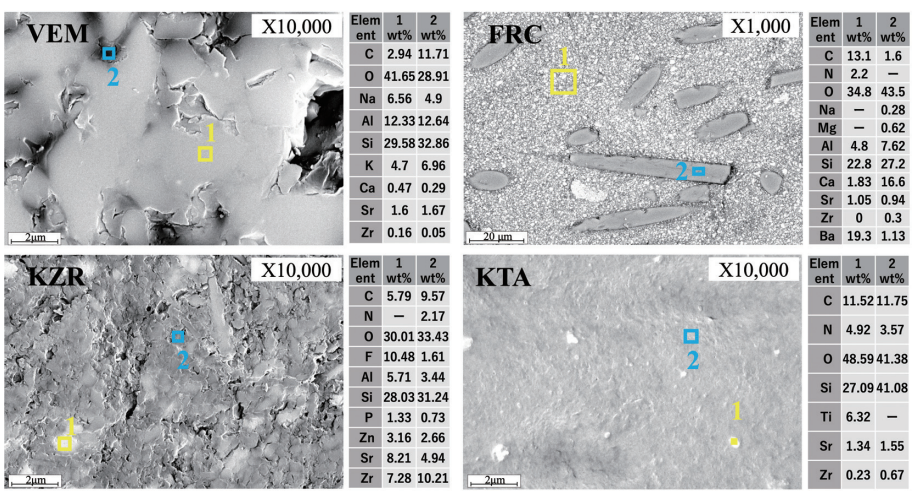

Element	1 wt%	2 wt%
C	2.94	11.71
O	41.65	28.91
Na	6.56	4.9
Al	12.33	12.64
Si	29.58	32.86
K	4.7	6.96
Ca	0.47	0.29
Sr	1.6	1.67
Zr	0.16	0.05

Element	1 wt%	2 wt%
C	13.1	1.6
N	2.2	–
O	34.8	43.5
Na	–	0.28
Mg	–	0.62
Al	4.8	7.62
Si	22.8	27.2
Ca	1.83	16.6
Sr	1.05	0.94
Zr	0	0.3
Ba	19.3	1.13

Element	1 wt%	2 wt%
C	5.79	9.57
N	–	2.17
O	30.01	33.43
F	10.48	1.61
Al	5.71	3.44
Si	28.03	31.24
P	1.33	0.73
Zn	3.16	2.66
Sr	8.21	4.94
Zr	7.28	10.21

Element	1 wt%	2 wt%
C	11.52	11.75
N	4.92	3.57
O	48.59	41.38
Si	27.09	41.08
Ti	6.32	–
Sr	1.34	1.55
Zr	0.23	0.67

Fig. 9 Elemental analysis of the filler/fiber and matrix narrow spot areas at 10,000× magnification for VEM, KZR, and KTA and 1,000× magnification for FRC, which were particularly characteristic.
At 20 kV, detector; EDX.

CAD-CAM materials were confirmed to have sufficient nanohardness and nano-reduced elastic modulus for use as restorative materials. This indicates their potential for application in the restorative full-crown treatment of deciduous teeth.

The nanohardness values of the FRC-matrix region and composite resin groups (KTA, KZR, C27, C30) (0.65–1.03 GPa) were significantly lower than that of DME (3.37 GPa) and about one-third that of IPS (3.63 GPa). If dentin repair is assumed necessary, the material must

behave similar to dentin. These FRC-matrix region and composite resin groups exhibited values similar to the nanohardness of 0.55 GPa of healthy dentin of deciduous teeth, as reported by Hosoya *et al.*[23]. Future studies based on dentin restorations are required. Interestingly, VEM-polymer exhibited significantly lower nanohardness and nano-reduced elastic modulus than VEM-ceramics. There were significant differences between the FRC-fiber and the FRC-fiber surrounding the matrix. The nanohardness and nano-reduced elastic modulus were measured separately for the horizontal cross-sections in the plane of the fiber from various angles of experimental FRC, but no significant difference by direction was found. The effectiveness of fiber reinforcement is determined by a variety of factors, including the resins used; the weight, orientation, and location of fibers; and the adhesion of fibers to the polymer matrix[24]. The development of FRC materials aims to enhance fracture toughness. This improves the mechanical properties of composite-based materials and reduces problems that may adversely affect clinical performance[12-14]. The nanohardness and nano-reduced elastic modulus of the FRC-fiber were considerably higher than those of the surrounding matrix in this study. However, the nanohardness and nano-reduced elastic modulus of the fiber surrounding the matrix and the elemental composition were identical to those of C27 and C30, suggesting that FRC can be used in the restorative full crown treatment of deciduous teeth. VEM is considered a polymer-infiltrated ceramic network (PICN), which consists of a dual-network structure of ceramic and resin skeletons[25]. In this study, VEM-ceramic exhibited a higher nanohardness and nano-reduced elastic modulus than the other composite resin groups. This might be attributed to the more robust microstructural geometry of PICN.

The nanohardness of the nanoindentation imprints used in this study depends on the applied load and indentation depth and is measured as a function of the applied load (P) and the size of the indentation contact area[26]. The nanohardness in previous studies was reported to be 4.03 GPa for permanent teeth and 3.1 GPa for VEM[27]. In this study, the nanohardness values of PME and VEM-ceramic were 4.34 GPa and 3.2, respectively, indicating that the measurement method was appropriate. Previous studies have reported a positive correlation between hardness and elastic modulus[27], revealing that the elastic modulus is also related to the stiffness of the material[28]. In the present study, a strong correlation (ρ=0.813, p<0.001) was observed between the nanohardness and nano-reduced elastic modulus of the CAD-CAM materials.

In this study, nanoindentation coupled with *in situ* SPM was conducted. Material pile-ups reflect local material softening and imply plastic deformation at the nanoscale[29]. In this study, the SPM images of the nanoindentation imprints showed that plastic pile-ups of approximately 7.7–138.01 nm occurred around the indentation contacts of all specimens. The CAD-CAM specimens exhibited a correlative tendency for harder materials to have smaller pile-up sizes. However, a hard but high pile-up was observed in the enamel of deciduous and permanent teeth. In particular, the pile-ups of deciduous teeth were greater than those in any other specimen, suggesting the plastic deformation of deciduous teeth.

Based on the SEM and EDS results obtained in this study, five types of structures were observed in the CAD-CAM block specimens. These include a resin matrix structure with a filler (KTA, PZB, KZR, C27, and C30), a resin matrix structure with a fiber and filler (FRC), a ceramic network structure (VEM), a ceramic structure (IPS), and a PMMA structure without a filler (PMM). The chemical properties of the CAD-CAM materials differed among the various materials, with C, O, and Si being the common elements detected, whereas the enamel was mainly composed of C, O, P, and Ca. In the EDS analysis of IPS, elements Mg, P, K, Zn, Zr, and Ce were detected characteristically, whereas Li was not detected, indicating that Li exists as nano size and is distributed below the limit of detection. Large amounts of Al and Si were found in both ceramics and polymers. SiO_2 and Al_2O_3 were the main components according to the manufacturer's instructions. KZR contains fillers such as fluorine sustained-release fillers, nanosized spherical fillers (SiO_2), ceramic cluster fillers, and aggregates of sub-micro-sized spherical fillers (SiO_2–ZrO_2–Al_2O_3)[30]. In addition to Si and Sr, large amounts of Zr and Zn were detected. This indicates that the spherical filler aggregates (SiO_2–ZrO_2–Al_2O_3) and ceramic cluster fillers were predominant. Spot analysis detected a large amount of F in the white filler areas. According to the manufacturer's information on KTA, the particle sizes of SiO_2 and Al_2O_3 are 40 nm and 20 nm; however, in this study, a large amount of Si was detected in the monomer, and no Al was detected. In addition, Ti was detected in the filler region, but not in the manufacturer's information. The composite resins used in this study, FRC, C27, and C30, were uniformly composed of small particles within 1 μm, and almost similar images were observed in all three. In C27 and C30, Ba, which was considered to have originated from barium glass, as declared by the manufacturer, was detected in higher amounts than in the other materials. Elements N, Mg, Cl, and Ca were detected in the FRC-fibers. PZB contained high amounts of Si, Sr, and Zr in the spherical filler, which likely originate from the zirconia-silica ceramic filler on the basis of the manufacturer's product description.

In this study, the Ca/P ratios for PME and DME were 1.67 and 1.79, respectively, which are close to those reported for PME (1.8) in a previous study[31]. Several studies on enamel organ development have shown that the Ca/P molar ratio varies for individual teeth, but is constant along the developing tooth organ[32-34]. Similarities were found between the EDS results achieved for the enamel in this study and those reported in previous studies[31].

In conclusion, various CAD-CAM materials were confirmed to have sufficient nanohardnesss, nano-reduced elastic modulus, and elemental and microstructural properties, indicating their potential

application in the restorative treatment of full crowns of deciduous teeth.

This study has several limitations. First, the nanoindentation test is sensitive to thermal changes, mechanical vibrations, and acoustic noise[26], and it is necessary to test the enamel and CAD-CAM specimens in the same environment. Second, only the nanohardness, nano-reduced elastic modulus, and elemental composition were analyzed in this study. To further investigate the relevance and durability of CAD-CAM materials in pediatric dental clinical applications, additional research must be conducted. The material wear and its effect on the wear of antagonistic deciduous teeth require further investigation, because deciduous teeth are characterized by natural wear during permanent tooth eruption. Third, nanoindentation testing could not be performed on the dentin because of humidity. Further studies are required to examine the mechanical and elemental properties of dentin.

ACKNOWLEDGMENTS

Authors are grateful to staff members in the department of Pediatric Dentistry/Special Needs Dentistry, Institute of Science Tokyo for support.

This study was funded by a Grant-in-Aid for Scientific Research [No. 24K13194 to K.W., 2024] offered by the Ministry of Education, Culture, Sports, Science, and Technology of Japan.

CONFLICTS OF INTEREST

P.V. declares that he is a consultant for the Stick Tech Member of GC Company in training, research, and development. The authors declare that they have no conflicts of interest.

REFERENCES

1) Gimenez T, Bispo BA, Souza DP, Viganó ME, Wanderley MT, Mendes FM, *et al.* Does the decline in caries prevalence of Latin American and Caribbean children continue in the new century? Evidence from systematic review with meta-analysis. PloS One 2016; 11: e0164903.
2) Wada K, Miyashin M, Nango N, Takagi Y. Wear of resin composites and primary enamel and their applicability to full crown restoration of primary molars. Am J Dent 2011; 24: 67-73.
3) Wada K, Miyashin M. New techniques for producing aesthetic, direct full-crown composite resin restorations for primary molars: A 24-month follow-up study of eight cases. Eur J Paediatr Dent 2015; 16: 205-209.
4) Holsinger DM, Wells MH, Scarbecz M, Donaldson M. Clinical evaluation and parental satisfaction with pediatric zirconia anterior crowns. Pediatr Dent 2016; 38: 192-197.
5) Bamdadian Z, Pasdar N, Alhavaz A, Ghasemi S, Bijani A. Comparative evaluation of physical and mechanical properties of different brands of primary molar stainless-steel crowns: An in vitro study. Open Access Maced J Med Sci 2019; 7: 4120-4126.
6) Walia T, Salami AA, Bashiri R, Hamoodi OM, Rashid F. A randomised controlled trial of three aesthetic full-coronal restorations in primary maxillary teeth. Eur J Paediatr Dent 2014; 15: 113-118.
7) Shin Y, Wada K, Tsuchida Y, Ijbara M, Ikeda M, Takahashi H, *et al.* Wear behavior of materials for additive manufacturing after simulated occlusion of deciduous dentition. J Mech Behav Biomed Mater 2023; 138: 105627.
8) Lauvahutanon S, Takahashi H, Shiozawa M, Iwasaki N, Asakawa Y, Oki M, *et al.* Mechanical properties of composite resin blocks for CAD/CAM. Dent Mater J 2014; 33: 705-710.
9) Rosentritt M, Krifka S, Strasser T, Preis V. Fracture force of CAD/CAM resin composite crowns after in vitro aging. Clin Oral Investig 2020; 24: 2395-2401.
10) Yamaguchi S, Kani R, Kawakami K, Tsuji M, Inoue S, Lee C, *et al.* Fatigue behavior and crack initiation of CAD/CAM resin composite molar crowns. Dent Mater 2018; 34: 1578-1584.
11) Wada K, Ikeda E, Wada J, Inoue G, Miyasaka M, Miyashin M. Wear characteristics of trimethylolpropane trimethacrylate filler-containing resins for the full crown restoration of primary molars. Dent Mater J 2016; 35: 585-593.
12) Mangoush E, Garoushi S, Vallittu PK, Lassila L. Influence of short fiber- reinforced composites on fracture resistance of single-structure restorations. Eur J Prosthodont Restor Dent 2020; 30; 28: 189-198.
13) Mangoush E, Lassila L, Vallittu PK, Garoushi S. Microstructure and surface characteristics of short- fiber reinforced CAD/CAM composite blocks. Eur J Prosthodont Restor Dent 2021; 29: 33508179.
14) Mangoush E, Lassila L, Vallittu PK, Garoushi S. Shear-bond strength and optical properties of short fiber-reinforced CAD/CAM composite blocks. Eur J Oral Sci 2021; 129: e12815.
15) Charlton DG, Roberts HW, Tiba A. Measurement of select physical and mechanical properties of 3 machinable ceramic materials. Quintessence Int 2008; 39: 573-579.
16) Della Bona A, Corazza PH, Zhang Y. Characterization of a polymer-infiltrated ceramic-network material. Dent Mater 2014; 30: 564-569.
17) Zhang Y, Kelly JR. Dental ceramics for restoration and metal veneering. Dent Clin North Am 2017; 61: 797-819.
18) Ijbara M, Wada K, Tabata MJ, Wada J, Inoue G, Miyashin M. Enamel microcracks induced by simulated occlusal wear in mature, immature, and deciduous teeth. Biomed Res Int 2018; 2018: 5658393.
19) Wada K, Ijbara M, Salim NA, Wada J, Iwamoto T. Three-dimensional microscopic comparison of wear behavior between immature and mature enamel: An in vitro study. BMC Oral Health 2023; 23: 40.
20) Iwata J, Asakura M, Hayashi T, Tsuruta S, Hori M, Nagase Y, *et al.* Leaching behaviors of computer-aided design/computer-aided manufacturing composite resin component elements immersed in water. J Prosthodont Res 2019; 63: 221-226.
21) Drummond JL, Khalaf MA, Randolph RG. In vitro aging of composite restorative materials. Clin Mater 1988; 3: 209-221.
22) Marshall Jr GW, Balooch M, Gallagher RR, Gansky SA, Marshall SJ. Mechanical properties of the dentinoenamel junction: AFM studies of nanohardness, elastic modulus, and fracture. J Biomed Mater Res 2001; 54: 87-95.
23) Hosoya Y, Marshall GW. The nano-hardness and elastic modulus of carious and sound primary canine dentin. Oper Dent 2004; 29: 142-149.
24) Jeng YR, Lin TT, Hsu HM, Chang HJ, Shieh DB. Human enamel rod presents anisotropic nanotribological properties. J Mech Behav Biomed Mater 2011; 4: 515-522.
25) Coldea A, Swain MV, Thiel N. Mechanical properties of polymer-infiltrated-ceramic-network materials. Dent Mater 2013; 29: 419-426.
26) Fischer-Cripps AC. Nanoindentation, Mechanical Engineering, New York, Springer New York, 2011.
27) Alamoush RA, Silikas N, Salim NA, Al-Nasrawi S,

Satterthwaite JD. Effect of the composition of CAD/CAM composite blocks on mechanical properties. Biomed Res Int 2018; 4893143.
28) Sakaguchi RL, Powers JM, editors. Craig's restorative dental materials. 13th ed. Philadelphia, Elsevier/Mosby. 2012.
29) Springall Gabriella AC, Yin Ling. Nano-scale mechanical behavior of pre-crystallized CAD/CAM zirconia-reinforced lithium silicate glass ceramic. J Mech Behav Biomed Mater 2018; 82: 35-44.
30) Yamazoe M, Kato T, Anraku T. Introduction of the features and performance evaluation of KZR-CAD HR Block2. J Jpn Soc Dent Prod 2015; 29: 19-27.
31) J.alevik B, Odelius H, Dietz W, Noren J. Secondary ion mass spectrometry and X-ray microanalysis of hypomineralized enamel in human permanent first molars. Arch Oral Biol 2001; 46: 239-247.
32) Deutsch D, Pe'er E. Development of enamel in human fetal teeth. J Dent Res 1982; 61: 1543-1551.
33) Sasaki T, Debrari K, Garant PR. Ameloblast modulation and changes in the Ca, P, and S content of developing enamel matrix revealed by SEM-EDX. J Dent Res 1987; 66: 778-783.
34) Kodaka T, Debari K, Yamada M, Kuroiwa M. Mineral content of the innermost enamel in erupted human teeth. J Electron Microsc 1991; 40: 19-23.